CHEMISTRY OF MATERIALS

Article

pubs.acs.org/cm

Possible *n*−type carrier sources in $In_2O_3(ZnO)_k$

Haowei Peng,*[,†] Jung-Hwan Song,[†] E. Mitchell Hopper,[‡] Qimin Zhu,[‡] Thomas O. Mason,[‡] and Arthur J. Freeman[†]

[†]Department of Physics and Astronomy, Northwestern University, Evanston, Illinois 60208, United States

[‡]Department of Materials Science and Engineering, Northwestern University, Evanston, Illinois 60208, United States

Supporting Information

ABSTRACT: Homologous compounds with the formula $In_2O_3(ZnO)_k$, where k is an integer, have potential applications as transparent conducting oxides and high temperature thermoelectric materials. In this study, we focus on the defect properties. Using the $k = 3$ phase as a prototype, we calculate with the first-principles method the defect formation energies and transition levels of the most probable *n*-type carrier producers, which include oxygen vacancy (V_O), indium antisite on zinc (In_{Zn}), indium interstitial (In_i), and zinc interstitial (Zn_i). The site-preference of these defects has been explored by comparing the total energies of defects at different sites. Under the *n*-type environment, In_{Zn} has a low formation energy and meanwhile a transition energy level close to the conduction band minimum (CBM); V_O also has a lower formation energy, however a deep transition energy level in the band gap; the cation interstitials have high formation energies, although their defect transition energy levels are quite shallow. Besides, we find that V_O and In_{Zn} tend to form a defect complex when the two isolated defects take the nearest-neighboring atomic sites in the same *ab*-plane. We conclude that In_{Zn} and its related defect-complex are the possible *n*−type carrier sources in $In_2O_3(ZnO)_k$. Besides, we found that V_O has a significant site-preference, which can modify the site-preference of In_{Zn} by forming defect-complexes. This may lead to high anisotropy in relaxation time, and then the experimentally reported strong anisotropy in electrical conductivities in $In_2O_3(ZnO)_5$.

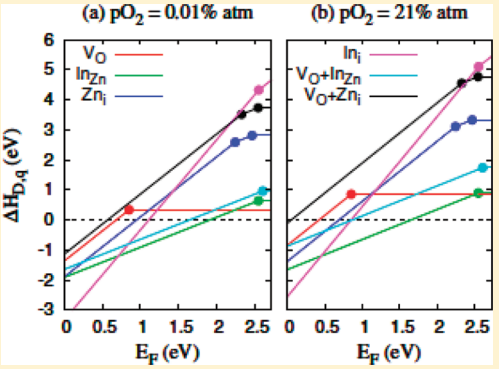

KEYWORDS: *$In_2O_3(ZnO)_k$, n-type defects, first-principles*

INTRODUCTION

The series of homologous In−Zn−O compounds with the formula $In_2O_3(ZnO)_k$, where k is an integer, have been studied extensively. This series has two important potential applications: as transparent conducting oxides (TCO) used in optoelectronic devices, and as thermoelectric (TE) materials for high temperature TE power generation. Until now, In_2O_3:Sn (ITO) is the most commonly used TCO owing to its high optical transparency of 85%-90% in the visible region associated with an electrical conductivity as high as 1000−5000 S/cm. Replacing In_2O_3 with $In_2O_3(ZnO)_k$ can largely reduce the cost by avoiding the heavy usage of expensive indium, and meanwhile retains the good electrical and optical properties.[1,2] Traditional high-temperature TE materials, including Si−Ge alloys, metal chalcogenides, transition metal disilicides, and B-based compounds, suffer from their chemical instability at elevated temperature. Compared with these materials, $In_2O_3(ZnO)_k$ has three advantages:[3] first, it possesses excellent structural and chemical stability even at high temperature; second, its wide band gap prevents the thermal excitation of carriers and thus allow the TE figure of merit, ZT, to continue to increase at high temperatures; the third, $In_2O_3(ZnO)_k$ has a low thermal conductivity due to its natural superlattice or layered structure.[15] Thus, $In_2O_3(ZnO)_k$ is a promising alternative to these traditional high-temperature thermoelectric materials.

For both the two potential applications of $In_2O_3(ZnO)_k$, the generation of charge carriers is of special importance. Like their parent binaries, In_2O_3 and ZnO, $In_2O_3(ZnO)_k$ shows an intrinsic *n*-type conducting behavior. To find out the carrier generation mechanism, using the first-principles method, we calculate the formation energies and defect transition energy levels[7] of several most possible *n*-type native defects in $In_2O_3(ZnO)_k$ under the experimental growth conditions.[3] In experiments, $In_2O_3(ZnO)_k$ shows strong anisotropic electrical conductivities; for example, the electrical conductivity of a *c*-axis oriented $In_2O_3(ZnO)_5$ thin film is 1 order of magnitude higher than that of an *ab*-plane oriented one,[4] and in the single crystal the conductivity along the *ab* plane is even 2 orders of magnitude larger than that along the *c* direction.[5] However, we found that the lowest conduction bands of the $k = 1$, 2, and 3 phases show similar dispersion in the three directions along the reciprocal lattice vectors, based on highly precise first-principles calculations using both the local density approximation (LDA) and screened-exchange LDA (sX-

Received: July 15, 2011
Revised: November 9, 2011
Published: November 15, 2011

   dx.doi.org/10.1021/cm202020g | *Chem. Mater.* 2012, 24, 106−114

LDA).[3] In this study, we find that this anisotropy is likely related to the spatial distribution of the defects.

Essentially, the atomic structure is the only necessary information for first-principles calculations. The atomic structures of $In_2O_3(ZnO)_k$ compounds are very complicated, which consist of (Zn/In)O slabs separated by single-edge-sharing In−O octahedral layers.[9−12] High-resolution transmission electron microscopy images show a modulated structure with zigzag features in the (Zn/In)O slabs.[9,13] Using first-principles calculations, Da Silva et.al.[14,15] investigated the formation mechanisms, and identified the ground-state crystal structures for $In_2O_3(ZnO)_k$ with k = 1−6. In Figure 1, we show the crystal structure of the

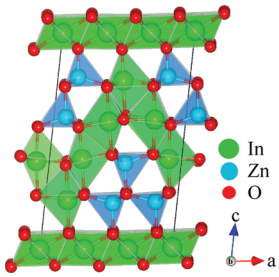

Figure 1. (Color-online) Crystal structure of $In_2O_3(ZnO)_3$, in the view where the zigzag boundary is shown.

k = 3 phase,[16] where the zigzag boundary is highlighted. The structural models in this study are those provided by Da Silva et.al.; for more details we refer to ref 15.

In the primitive cells of the $In_2O_3(ZnO)_k$ with k = 1−6, there are 28, 72, 66, 208, 150, and 408 atoms respectively,[15] among which the k = 3 phase is chosen as a prototype for defect calculations based on the following considerations: (1) the k = 1 phase, to our knowledge, has not been successfully synthesized; (2) the k = 2 phase is unstable in bulk form below 1550 °C;[17] (3) $In_2O_3(ZnO)_k$ with k = 1 and 2 have much less complicated structures than those with k > 2; (4) the phases with k = 4, 5, and 6 have large unit cells, which are very computational expensive for defect calculations with a supercell approach in this study; (5) the zigzag-shaped inversion domain boundary[14,15] is already perfectly shown in the phase with k = 3 as in phases with a larger k. In addition, because of the structure similarity, we believe that our results based on the k = 3 phase can be generalized to other phases, and also shed some light on other homologous $InMO_3(ZnO)_k$ (M = Ga, and Al) compounds.[15]

Even choosing the k = 3 phase as a prototype, which has a moderate size (66 atoms per unit cell), we still cannot calculate extensively all possible defects due to the extremely low symmetry and complicated structure. Fortunately, we can take lessons from quite a lot of previous studies on the intrinsic n-type behavior in In_2O_3 and ZnO.[18,19,21−31] Although controversy exists, a general conclusion is that oxygen vacancy (V_O) and cation interstitials (Zn_i or In_i) are the most probable sources of n-type charge carrier.[18,19,21−28] Inspired by these works, V_O, In_i, and Zn_i should be considered as possible n-type carrier sources in $In_2O_3(ZnO)_k$. Besides, during the high-temperature solid state reaction,[3,34] the $In_2O_3(ZnO)_k$ may experience zinc-loss due to vaporization. Thus, the cation antisite defect, indium on zinc (In_{Zn}), also should be considered. For binaries, V_O-Zn_i defect complex in ZnO,[30] and V_O-In_i in In_2O_3[29,31] are proposed to be the origin of n-type conductivity in undoped ZnO and In_2O_3. To check this possibility, we also calculated the defect-complexes between the isolated V_O and other three kinds of cation-related defects, which have low formation energies.

For defect calculations, we also need information about the competing phases. For the series of homologous $In_2O_3(ZnO)_k$ compounds, this is a difficult problem without help from experiments, because there are so many phases (k = 2−9, 11, 13, 15, and 20)[17,32−34] composed of In−Zn−O elements, and the crystal structures of some of them are still unknown. T. Moriga et.al.[34] determined the equilibrium phase relationships between 1100 and 1400 °C in the ZnO-In_2O_3 system, and demonstrated that the phases with k = 4 and 5 are the two ternary secondary-phases for the k = 3 phase.

In the next sections, we first describe the calculation method; and then present our results and discussions, which is followed by a brief summary.

METHOD OF CALCULATIONS

Technical Details. Our calculations were based on the density functional theory within the Perdew-Burke-Ernzerhof (PBE) generalized gradient approximation (GGA).[37] The electron-ion interaction was described by pseudopotentials generated with the projector-augmented-wave (PAW) method,[38] as implemented in the Vienna Ab-initio Simulation Package (VASP).[39] Zn 3d and In 4d electrons were treated as valence electrons. The electronic wave functions were expanded with plane waves up to a kinetic energy of 450 eV. For Brillouin-zone integration, a Γ-centered 2 × 4 × 2 Monkhost-Pack[40] k-mesh was used for $In_2O_3(ZnO)_3$ 66-atom primitive cell,[15] and k-meshes with a similar quality for $In_2O_3(ZnO)_k$ with k = 4 and 5. For the 1 × 2 × 1 132-atom supercells, a 2 × 2 × 2 Monkhost-Pack k-mesh was employed. Convergence with respect to both the plane-wave cutoff energy and k-mesh has been checked. All the primitive cells were fully relaxed until the residual atomic forces were less than 0.01 eV/Å. To save the computational cost, we relaxed the supercells until the residual atomic forces were less than 0.03 eV/Å, but we found the force on most atoms was already less than 0.01 eV/Å.

Defect Formation Energy and Transition Level. In the standard approach for first-principles defect calculations, the defect system is modeled using a supercell.[7,8] A defect or defect-complex is put in a periodic supercell, and a uniform background charge is added to keep the whole supercell in charge neutral for a charged defect. The formation energy of a defect D in a charge state q is defined as[7,24]

$$\Delta H_{D,q}(E_F, \mu) = E_{D,q} - E_H + \sum n_\alpha(\mu_\alpha^0 + \Delta\mu_\alpha) + q(E_V + E_F) \quad (1)$$

where $E_{D,q}$ and E_H are the total energies of the host+defect and host-only supercells, respectively; μ_α^0 is the elemental reference energy of element α, which can be calculated from the ground-state elemental crystal or gas molecular; $\Delta\mu_\alpha$ is the chemical potential of element α with respect to μ_α^0; E_V is the energy of the valence band maximum (VBM) of the host system; E_F is the Fermi level with respect to E_V; n_α is the number of α elements, and q is the number of electrons transferred from the supercell to the corresponding reservoirs in forming the host+defect supercell. The defect transition energy level $\varepsilon(q/q')$ between charge states q and q' of the defect D is defined as the Fermi level, E_F, at which

dx.doi.org/10.1021/cm202020g | Chem. Mater. 2012, 24, 106−114

$\Delta H_{D,q}(E_F,\mu)=\Delta H_{D,q'}(E_F,\mu)$:

$$\varepsilon(q/q') = [\Delta H_{D,q}(E_V, \mu) - \Delta H_{D,q'}(E_V, \mu)]/(q' - q) \quad (2)$$

where $\varepsilon(q/q')$ is also defined with respect to E_V, as the same as E_F.

The defect formation energy and transition energy level calculated using the above method needs some corrections because of the notorious LDA/GGA band gap-error, and the finite-size supercell approach.[24,41] Here we choose the correction methods proposed by S. Lany and A. Zunger,[24] which include (i) band-edge correction using the GGA+U method, (ii) shifting shallow levels with corresponding host band edges, (iii) band-filling correction, (iv) potential-alignment correction for supercells with a charged defect, and (v) image charge correction for charged defects. For the band-edge correction, we chose the rotational invariant LDA/GGA +U method[42] with U = 4.8 eV, and 6.0 eV for the semicore d states of In and Zn, respectively, and with J = 0.0 eV for both. The band gap of 2.72 eV reported by recent experiment[3] is used, which results in a downward-shifting of the valence bands by 0.32 eV, and an upward-shifting of the conduction bands by 1.70 eV. For the potential-alignment, we chose the 1s core-level of the atoms farthest away from the defect site as an energy reference.[7,41] For the image charge correction, we chose the simplified Makov-Payne scheme as shown in eq (24) in ref 24. The static dielectric constant was set to 8.32 which is the weighted average of the static dielectric constants of ZnO[43] and In_2O_3.[44]

In principle, methods beyond DFT, like the GW method,[45] should be used to avoid the LDA/GGA errors, however, these kinds of calculations are too computationally demanding for the present system. The finite-size error in the supercell approach can also be avoided if new methods are emplyed, for example, the embedded cluster approach[46] where no periodic boundary condition is needed. Besides, instead of the zero-temperature total energies in eq 1, the Gibbs free energies are needed for accurately prediction of defects in high temperature.[47] However, neglecting the other terms should not result in a qualitative change in the results as argued by Van de Walle *et.al.*[8]

Available Elemental Chemical Potentials. As shown in eq 1, the formation energy is not a constant, but a function of elemental chemical potentials and Fermi level (or chemical potential of electrons). The Fermi level is usually defined between the VBM and conduction band minimum (CBM) of the pristine host; the range of elemental chemical potentials are limited by the following constraints:

i, the elemental chemical potentials should have the values that maintain a stable $In_2O_3(ZnO)_3$ host, which requires

$$2\Delta\mu_{In} + 3\Delta\mu_{Zn} + 6\Delta\mu_{O} = \Delta H_f[In_2O_3(ZnO)_3] \quad (3)$$

where the heat of formation of $In_2O_3(ZnO)_3$ is defined as $\Delta H_f[In_2O_3(ZnO)_3]=E[In_2O_3(ZnO)_3]-2\,\mu^0_{In} - 3\,\mu^0_{Zn} - 6\,\mu^0_{O}$, and similar definitions are applied to other compounds below.

ii, the precipitation of the elements In, Zn, and O should not happen, which requires

$$\Delta\mu_{In} \le 0;\ \Delta\mu_{Zn} \le 0;\ \Delta\mu_{O} \le 0 \quad (4)$$

iii, the precipitation of secondary-phase binaries In_2O_3 and ZnO should not happen, which requires

$$2\Delta\mu_{In} + 3\Delta\mu_{O} \le \Delta H_f(In_2O_3) \quad (5)$$

$$\Delta\mu_{Zn} + \Delta\mu_{O} \le \Delta H_f(ZnO) \quad (6)$$

iv, the precipitation of secondary-phase ternaries, as mentioned in Introduction, $In_2O_3(ZnO)_4$ and $In_2O_3(ZnO)_5$ should not happen, which requires

$$2\Delta\mu_{In} + 4\Delta\mu_{Zn} + 7\Delta\mu_{O} = \Delta H_f[In_2O_3(ZnO)_4] \quad (7)$$

$$2\Delta\mu_{In} + 5\Delta\mu_{Zn} + 8\Delta\mu_{O} = \Delta H_f[In_2O_3(ZnO)_5] \quad (8)$$

Density functional theory is a zero-temperature theory, so the above equations and inequalities are correct at zero-temperature. But when the entropy term $T\Delta S$ plays an important role, we have to replace the heat of formations (change of total energies) with the change of Gibbs free energies.[26] For $In_2O_3(ZnO)_k$ compounds with k = 1−5, we found

$$\Delta H_f[In_2O_3(ZnO)_k] > \Delta H_f(In_2O_3) + k\Delta H_f(ZnO) \quad (9)$$

and the energy differences between the left side and right side of eq 9 are around 0.25 eV per formula unit. As k increases from 1 to 5, the energy difference per atom decreases, and correspondingly the growth becomes easier in experiments.[34] However, although these ternary phases are found to be metastable with respect to their parent binaries, some of them can remain stable at low temperatures due to the kinetic barriers. Similar phenomenon was also reported in cases of $CuBO_2$[48] and $(GeTe)_m(Sb_2Te_3)_n$.[49]

Back to defect calculations, eq 9 results in the absence of available elemental chemical potentials which allow the formation of $In_2O_3(ZnO)_k$ without any secondary phases. In this case, the related entropy term is crucial. However, direct calculation of entropy from first-principles is not easily feasible here for the complicated oxides; instead of that, we turn to experimental data for help. From the experiments,[34,35] we know that the equilibrium or quasi-equilibrium solid state reactions

$$In_2O_3 + 5ZnO \rightarrow In_2O_3(ZnO)_5 \quad (10)$$

$$In_2O_3 + 4In_2O_3(ZnO)_5 \rightarrow 5In_2O_3(ZnO)_4 \quad (11)$$

$$In_2O_3 + 3In_2O_3(ZnO)_4 \rightarrow 4In_2O_3(ZnO)_3 \quad (12)$$

start at T^5_{low} = 1073K,[35] T^4_{low} = 1473K,[34] and T^3_{low} = 1531K,[34] respectively. Now, we define $\delta S_k=S[In_2O_3(ZnO)_k]-S(In_2O_3)-kS(ZnO)$, and assume δS_k to be a constant during the temperature range from 1073K to 1573K (the growth-temperature, T_g, in our experiments[3]). This assumption is reasonable because entropy increases slowly at high temperature, and partially canceling could be expected due to the definition of δS_k. Then, with respect to eq 10−eq 12, we have correspondingly

$$\Delta H[In_2O_3(ZnO)_5] - \Delta H(In_2O_3) - 5\Delta H(ZnO) = T^5_{low} \times \delta S_5 \quad (13)$$

$$4\Delta H[In_2O_3(ZnO)_5] + \Delta H(In_2O_3) - 5\Delta H[In_2O_3(ZnO)_4] = 4T^4_{low} \times \delta S_5 - 5T^4_{low} \times \delta S_4 \quad (14)$$

$$3\Delta H[In_2O_3(ZnO)_4] + \Delta H(In_2O_3) - 4\Delta H[In_2O_3(ZnO)_3] = 3T^3_{low} \times \delta S_4 - 4T^3_{low} \times \delta S_3 \quad (15)$$

dx.doi.org/10.1021/cm202020g | Chem. Mater. 2012, 24, 106−114

Solving the equation set, we can obtain the values of δS_3, δS_4, and δS_5. Then, we replace $\Delta H[In_2O_3(ZnO)_k]$ in eq 3, eq 7, and eq 8 with $\{\Delta H[In_2O_3(ZnO)_k]-T_g\delta S_k\}$, to mimic the growth conditions of the experiments.[3] Finally, the available range for the elemental chemical potentials are projected onto the $\Delta\mu_{Zn}-\Delta\mu_{In}$ plane, as shown in Figure 2.

As shown in Figure 2, given the growth conditions (temperature T_g, oxygen partial pressure pO_2, etc.), the chemical potentials of indium and zinc have only an extremely narrow range, which means the ration between indium and zinc should be almost a constant to produce $In_2O_3(ZnO)_3$ without other secondary phases, in agreement with the experimental line-shape phase diagram.[34] Figure 2 also shows that the main

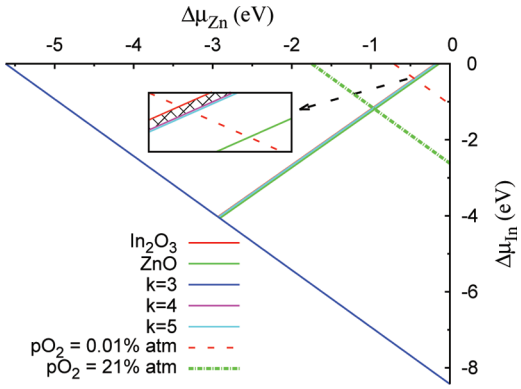

Figure 2. (Color-online) Available elemental chemical potentials for $In_2O_3(ZnO)_3$ as projected on the $\Delta\mu_{Zn}-\Delta\mu_{In}$ plane and indicated by filled patterns in the inset, which is blown up by more than 50 times compared to the original figure.

secondary phases are In_2O_3 and $In_2O_3(ZnO)_4$, which also agree with the experiment.[34] These agreements justify our procedure to some extent in a self-consistent manner.

The chemical potential of oxygen at the experimental condition were calculated based on the ideal gas theory, by which we can include the enthalpy and entropy contribution to $\Delta\mu_O$ in the O_2 gas phase at temperature T_g and partial pressure pO_2.[50] In our experiments,[3] T_g = 1573 K, and pO_2 = 0.01% *atm* and 21% *atm* for O-poor and O-rich conditions, the corresponding chemical potentials are denoted with the dashed lines in Figure 2.

In the above procedure, we ignore the entropy difference between Zn and ZnO, and that between In and In_2O_3, because the corresponding entropy terms are small compared with the heat of formation of $In_2O_3(ZnO)_k$, and also because they will only shift all the lines in Figure 2 as a whole along the axes. Thus, further considerations will not affect our conclusions in a significant way.

RESULTS AND DISCUSSION

There are totally 66 atoms in the monoclinic primitive cell of $In_2O_3(ZnO)_3$, including 12 indium, 18 zinc, and 36 oxygen atoms, as shown in Figure 3(a). For convenience, we labeled the atomic sites in the primitive cell: numbers 1−12, 13−30, and 31−66 are assigned to indium, zinc, and oxygen atoms, respectively; and starting from the front left bottom conner, the numbers increases at first from front to back (*b*-direction), then from left to right (*a*-direction), and then from bottom to top (*c*-direction). Some atomic sites which will be mentioned frequently in the following are already explicitly labeled in

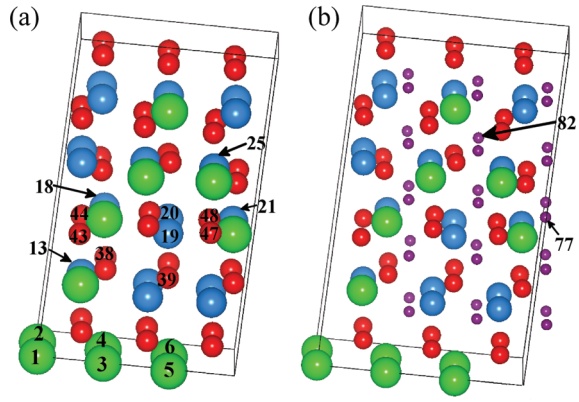

Figure 3. (Color-online) (a) Atomic sites and (b) interstitial sites in the $In_2O_3(ZnO)_3$ primitive cell. Same legends in Figure Figure 1 are used, and in (b) the purple spheres are used to represent the interstitial sites. For convenience, we labeled some sites with numbers, and refer these sites in the format of O48 which means the oxygen site labeled with the number 48.

Figure 3(a). Because of the low symmetry, all the atomic sites in the primitive cell are inequivalent to each other, and to investigate the spatial distributions (or site-preference) of the defects, we should essentially explore all the possible sites. Instead of that, we managed to classify the atomic sites according to several criteria described below, which reduced the computational cost by a factor of 2/3.

As shown in Figure 1, the structure units of $In_2O_3(ZnO)_3$ include the In−O octahedron in the In−O layers, Zn−O tetrahedron, In−O bipyramid in the (In/Zn)O slab, and Zn−O bipyramid which is behind the In−O bipyramid in Figure 1. Correspondingly, we call the cation ions In(6), Zn(4), In(5), and Zn(5), respectively, where the numbers in parentheses indicate the coordination numbers. By contrast, all the oxygen atoms are 4-fold coordinated, however, with different local environments which can be derived from the first criterion. For example, O39 (the oxygen atom labeled with the number 39) is surrounded by four Zn(4) atoms, while O44 is surrounded by two Zn(5) and two In(5) atoms. Besides, the distance from the atomic site to the In−O layer along the *c*-direction is a natural criterion. For oxygen sites, O44 is a special case due to a Zn−O with a bond-length of 2.64 Å, which distinguishes O44 from O43. For the zinc sites, we should be more careful. In $In_2O_3(ZnO)_k$, oxygen atoms in the (In/Zn)O slab satisfy the electron octet rule in two different ways:[15] one is that the single oxygen atom by itself obtains two electrons from its surrounding cations; the other is that two oxygen atoms forming an oxygen pair, e.g., O47 and O48, obtain four electrons from their surrounding cations. Because this directly relates to the distribution of electron charge density, we further distinguish Zn19 from Zn20, and Zn18 from Zn21. Using this procedure, we determined 6 kinds of "quasi-inequivalent" zinc sites and 12 kinds of "quasi-inequivalent" oxygen sites. This classification scheme turns out to be quite efficient; the total-energy difference between defects which are located at two "quasi-equivalent" sites is smaller than 5 meV based on several test calculations.

In Figure 3(b) we show the cation interstitial sites in $In_2O_3(ZnO)_3$ which are located at the centers of the largest empty-spheres in the anion sublattice. There are totally 30 interstitial sites which are inequivalent, but we determined 13 kinds of "quasi-inequivalent" sites for Zn_i or In_i using the same classification procedure.

dx.doi.org/10.1021/cm202020g | *Chem. Mater.* 2012, 24, 106−114

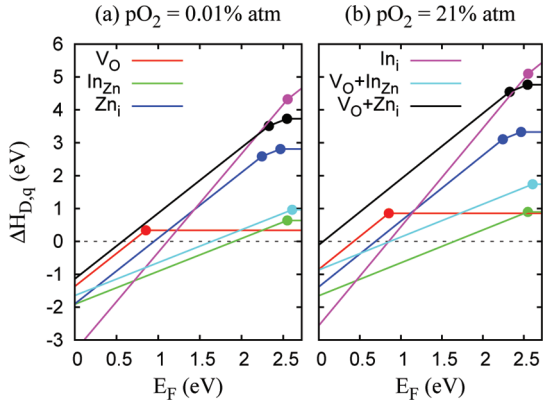

Figure 4. (Color-online) Formation energies of various *n*-type defects and defect-complexes in $In_2O_3(ZnO)_3$ at growth-temperature T_g = 1573 K, and oxygen pressure (a) pO_2 = 0.01% and (b) pO_2 = 21% atm.

In Figure 4, we plot the formation energies of defects V_O at O48, In_{Zn} at Zn13, Zn_i at i82 (the interstitial site labeled with the number 82), and In_i at i77, and defect-complexes between the V_O at O48 and In_{Zn} at Zn21, and V_O at O48 and Zn_i at i77. These defects or defect-complexes have the lowest or second lowest formation energies compared with other defects of the same sort. In the *n*-type environment, where the Fermi level is close to the CBM, zinc interstitials and indium interstitials have formation energies about 2.0−4.0 eV higher than those of oxygen vacancies and indium antisite on zinc, so we will not discuss them any more. We also find that it does not tend to form complexes between zinc interstitials and oxygen vacancies, in contrast to what happens in ZnO.[30] So, we also ignore these defect complexes, and below we focus on oxygen vacancies (V_O), indium antisite on zinc (In_{Zn}), and the defect-complexes between them.

Oxygen Vacancies: V_O. In Table 1 we list the number of "quasi-equivalent" sites (n_{eq}), total energies in the neutral charge state with respect to that of V_O at site O48 (δE_{tot}), and defect transition energy levels [$\varepsilon(2+/0)$] of oxygen vacancies at 12 kinds of "quasi-inequivalent" oxygen sites. δE_{tot} is the same as the formation energy difference between oxygen vacancies located at O48 and other oxygen sites, so it is easy to draw similar lines for oxygen vacancies at sites other than O48 in Figure 4 with the values of δE_{tot} and $\varepsilon(2+/0)$. As shown in the table, δE_{tot}, and therefore, the formation energy differences vary from −0.20 to about 0.94 eV. Because the concentration of defects is in proportion to $n_{eq}\cdot exp(-\Delta H/k_BT)$, strong anisotropy should be expected for the spatial distribution of oxygen vacancies. Using the growth-temperature T_g = 1573 K, given the same n_{eq}, a δE_{tot} of about 0.3 eV corresponds to a difference in the concentration of about 1 order of magnitude. Thus, we can safely ignore the occurrence of oxygen vacancies at sites O31, O32, O33, O37, O39, O41, and O45.

What is the physical reason for this anisotropy? In the natural oxides of zinc and indium, zinc and indium atoms are usually 4-fold and 6-fold coordinated, respectively. The Zn−O and In−O bipyramid structure units can be regarded as sources of instability in $In_2O_3(ZnO)_k$. In Table 1, we also tabulated the local environment of these oxygen sites, and indeed, the vacancies at oxygen sites with more Zn(5) or In(5) nearest-neighbors generally have lower formation energies. O31, O32, and O33 are the oxygen sites belonging to the In−O octahedral layer, and it is difficult to create a vacancy at these sites because of the tightly correlated structure. Site O39 is very similar to the

Table 1. Numbers of "quasi-equivalents" sites (n_{eq}), fraction coordinates in *c*-direction (z), nearest neighbours, total energies in the neutral charge state with respect to that of V_O at O48 (δE_{tot}), and defect transition energy levels [$\varepsilon(2+/0)$] of oxygen vacancies at different atomic sites as shown in Figure 3(a)

Site label	n_{eq}	z	Nearest neighbors	δE_{tot} (eV)	$\varepsilon(2+/0)$ (eV)
48	2	0.429	In(5)+2 × Zn(5)[a]+Zn(4)	0.0	0.85
44	2	0.400	2 × In(5)+2 × Zn(5)[a]	−0.20	0.63
43	2	0.386	2 × In(5)[a]+2 × Zn(5)	0.30	0.93
38	2	0.250	In(5)+2 × Zn(5)[a]+Zn(4)	0.30	1.22
47	2	0.431	2 × In(5)[a]+Zn(5)+Zn(4)	0.33	0.97
37	2	0.252	2 × In(5)[a]+Zn(5)+Zn(4)	0.67	N/A
41	4	0.251	2 × In(5)[a]+Zn(5)+Zn(4)	0.80	N/A
39	4	0.247	4 × Zn(4)	0.89	1.61
45	4	0.431	In(5)[a]+Zn(5)+2 × Zn(4)	0.94	N/A
32	2	0.076	3 × In(6)+Zn(5)	0.78	N/A
31	2	0.076	3 × In(6)+In(5)	0.88	N/A
33	8	0.069	3 × In(6)+Zn(4)	0.94	N/A

[a]The apical nearest neighbor which forms a cation-oxygen bond perpendicular to the oxygen basal plane.

oxygen sites in Wurtzite ZnO, surrounded by four Zn(4) atoms. For this site, we calculate the value of $[E_{tot}(\text{Host}+V_O)-E_{tot}(\text{Host})+E_{tot}(O_2)/2]$ for a 72-atom ZnO system and also the 132-atom $In_2O_3(ZnO)_3$, and the difference is only about 0.05 eV. (This also helps to justify our classification method according to the local environment.) For other eight kinds of oxygen sites, we also indicated in Table 1 the apical cation which is located out of the oxygen basal plane. Typically, the oxygen sites with Zn(5) as an apical cation have much lower formation energy than those with In(5) as an apical cation, given the same other conditions. This is also related the trend that zinc tends to form a Zn−O tetrahedron. When the oxygen vacancy is created, the apical Zn(5) or In(5) atom is pushed away from the vacancy site, while the in-plane Zn(5) or In(5) atom will relax toward the vacancy site; then, the apical (or in-plane) cation will form a distorted tetrahedron (or see-sawed) structure with their remained four nearest-neighboring oxygen atoms. The tetrahedron structure is favored by zinc but not by indium, so oxygen vacancies at sites O48, O44, and O38 which have an apical Zn(5) nearest neighbor are more stable than those at sites O47, O43, and O37, respectively, which have an apical In(5) nearest neighbors. Site O45 is an exception whose apical In(5) atom actually relaxes toward the vacancy site, resulting in an extremely high total energy. We compared the total energies of structures with or without relaxation: for the vacancy at site O45, the relaxation only reduces the total energy by 0.10 eV, while in other cases, the relaxation energy gain ranges from 0.30 to 0.61 eV. As another special case, the oxygen vacancy at site O44 has the lowest total energy, which should be related to the unusual long bond-length of about 2.6 Å between sites O44 and Zn13.

Here we summarize the rules of the anisotropic spatial distribution or site-preference of the oxygen vacancies in $In_2O_3(ZnO)_3$. First, oxygen vacancies are difficult to form in the In−O layer. Second, vacancies should tend to form at the oxygen sites along the zigzag boundary in the (Zn/In)O slab because all the Zn(5) and In(5) atoms occur there. Third, an oxygen vacancy with Zn(5) atom as the apical nearest neighbor should have a lower formation energy than that with an In(5)

dx.doi.org/10.1021/cm202020g | Chem. Mater. 2012, 24, 106−114

one. By carefully inspecting the structures of $In_2O_3(ZnO)_k$ with $k = 1-6$,[51] we found that the classification of 12 kinds of oxygen vacancies is also suitable for other phases. For example, in phases with $k = 4$, 5, and 6, we also found sites like O43 and O44 which is located at the V-shaped corner of the zigzag boundary in the second (Zn/In)O atomic layer, and sites like O47 and O48 pairs which are located in the second, third, etc. (Zn/In)O atomic layers. Notice that the counting of the (Zn/In)O atomic layers should start from both the top and bottom In−O layers. Because of the similarity between their structures, we believe that similar rules, especially the first two, can also be applied to the spatial distributions of oxygen vacancies in different phases with different k.

As shown in Figure 4, oxygen vacancies in $In_2O_3(ZnO)_3$ are negative-U systems, which is indicated by the quite large relaxation when the charge state q changes from 0 to 2+. For the charge state $q = 0$, most of the nearest neighboring cations relax inward by 5−10%, while for charge state $q = 2+$, most of the nearest neighboring cations relax outward by 20−32%, both with respect to the pristine supercell. The change of the relaxation is also reflected by the defect transition energy level $\varepsilon(2+/0)$. Basically, the larger the relaxation, the higher the transition energy level. Anyhow, for all the oxygen vacancies, $\varepsilon(2+/0)$ is very deep in the band gap, so the oxygen vacancies are not the n-type carrier source, as indicated by the experiments.[2,34]

Indium Antisite on Zinc: In_{Zn}. In Table 2, we list the δE_{tot} (total energies with respect to that of In_{Zn} at site Zn13) and defect transition energy levels $\varepsilon(1+/0)$ of six kinds of In_{Zn} antisite defects in $In_2O_3(ZnO)_3$. The defect formation energies of these defects with respect to that of In_{Zn} at site Zn13 are only slightly different from δE_{tot} due to the corrections[24] mentioned in Method of Calculations. Unlike the oxygen vacancies, there is no strong anisotropy in the spatial distribution, and the defect transition energy levels of all In_{Zn} are about 0.17 eV below the CBM, which is necessarily shallow for an n-type charge carrier producer.

Table 2. Numbers of "quasi-equivalent" sites (n_{eq}), fraction coordinates in c-direction (z), total energies in the neutral charge state with respect to that of In_{Zn} at site Zn13 (δE_{tot}), and defect transition energy levels [$\varepsilon(1+/0)$] of In_{Zn} at different atomic sites as shown in Figure 3(a)

Site label	n_{eq}	z	δE_{tot} (eV)	$\varepsilon(1+/0)$ (eV)
13	2	0.217	0.0	2.55
14	8	0.207	0.24	2.55
18	2	0.405	0.25	2.55
19	2	0.387	0.45	2.55
20	2	0.391	0.17	2.55
21	2	0.405	0.18	2.55

Sites Zn13, Zn18, and Zn21 are occupied by Zn(5) atoms in the perfect host structure. When an indium atom replaces these zinc atoms, the original bipyramid structure is strongly enhanced. Because indium is larger than zinc, the in-plane nearest oxygen atoms are squeezed outward by about 5% during the relaxation, however, the apical oxygen atoms will be attracted toward the substitutional indium atom by about 5% or more. Compared with zinc, indium is more likely to stay in a high-coordination environment. Especially, after an indium takes the site Zn13, the apical oxygen atom at site O44 shifts from 2.64 Å away to 2.34 Å away. The enhancement of the In−O bipyramid even happens to the zinc site originally with a Zn−O tetrahedron structure: when site Zn20 was occupied by an indium atom, the original 4-fold coordinated zinc site becomes a five coordinated indium site, with the oxygen atom at site O52 (quasi-equivalent to O44) shifting from 2.96 Å away to 2.36 Å away, with a displacement as large as 0.60 Å. Between the other two kinds of 4-fold coordinated zinc sites, In_{Zn} at site Zn14 has moderate formation energy, and In_{Zn} at site Zn19 has a quite higher formation energy. For all the In_{Zn} defect, when the charge state q changed from 0 to 1+, we only find a very slight relaxation, and we believe this is why all the In_{Zn} defects at different sites have the same defect transition energy level.

Now let us go back to Figure 4(a) and (b). At the growth-temperature, 1573K, when the oxygen partial pressure increases from 0.01% to 21% atm, the elemental chemical potentials of oxygen, indium, and zinc change from −2.46, −0.35, and −0.48 eV to −1.94, −1.13, and −1.00 eV, respectively. From eq 1, the formation energies of V_O increases by the amount of the change of $\delta\mu_O$, while the formation energy of In_{Zn} increases by the amount of the change of $[\delta\mu_{Zn}-\delta\mu_{In}]$. Thus, when the oxygen partial pressure increases, the formation energy of In_{Zn} increases about 50% slower than that of V_O. The experimentally observed relationship between the conductivity and partial oxygen pressure cannot be explained by regarding V_O as the main source of conductivity.[2,34] Combined with the previous conclusion that oxygen vacancies should not be the carrier producers, our calculations shed some light on this issue.

Defect Complexes between V_O and In_{Zn}. We usually consider defect-complexes between donor and acceptor, because of the attractive Coulomb interaction. However, the defect-complex between two donors can also happen, and the mechanism is schematically shown in Figure 5 (a) and (b). Let us consider two isolated donors, D1 and D2, among which the D2 state at a higher energy is either partially occupied as in Figure 5 (a) or fully unoccupied as in Figure 5 (b). When the two isolated donors are close enough to each other, hybridization between them can occur if symmetry allows. Then, the hybridization should result in a bonding state in a lower energy and an antibonding state in a higher energy, and the whole system obtain energy gain during this process because of the partially occupied or fully unoccupied antibonding state.

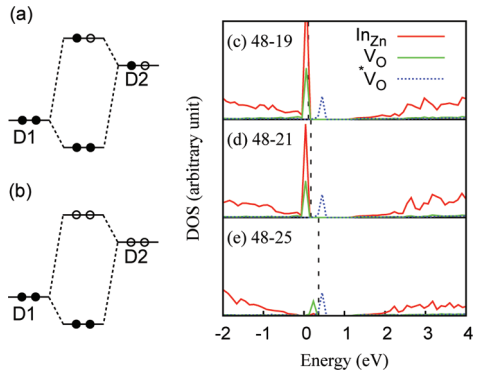

Figure 5. (Color-online) Schematic diagram of the attractive donor−donor interaction, where the D2 state is (a) partially or (b) fully unoccupied, and the site-projected densities of states (PDOS) on the In_{Zn} and V_O sites in systems including defect-complex between oxygen vacancy at site O48 and antisite In_{Zn} at (c) sites Zn18, (d) Zn21, and (e) Zn25. The PDOS of the isolated oxygen vacancy $^*V_O$ is also plotted as a reference.

dx.doi.org/10.1021/cm202020g | Chem. Mater. 2012, 24, 106−114

If the energy gain is larger than the energy loss due to the structure relaxation, defect complex between such two donors will occur. In ZnO[30] and In_2O_3,[29,31] this kind of attractive interactions are found between oxygen vacancies and zinc interstitials or indium interstitials. In this study, we first considered 7 kinds of defect-complexes between oxygen vacancies and zinc interstitials with low formation energies, however, we did not find significant energy gain. Below, we will focus on the defect-complexes between oxygen vacancies and indium antisite on zinc sites.

Here we define the binding energy, E_b, between two donors as $E_b(D1,D2)=\Delta H_{D1}+\Delta H_{D2}-\Delta H_{D1+D2}$. A positive, or negative, E_b implies the tendency for D1 and D2 to form, or not to form, a defect complex, and the complex is more stable if the positive E_b is larger. Because the donor−donor interaction becomes weaker when the distance between two donors decreases, and the largest positive binding energy in ZnO is around 0.52 eV,[30] we considered the defect-complex between the isolated V_O and In_{Zn} which are nearest-neighbors, and which already have relatively low formation energies. The results are shown in Table 3, where we tabulated the total energies and binding energies of 11 V_O−In_{Zn} defect-complexes in charge states $q = 0$ and +1. For all the defect-complexes, $E_b(q = 0)$ is always about 45−60 meV larger than $E_b(q=+1)$; this is reasonable as shown in Figure 5(a) and (b) which correspond to $q = 0$ and +1, respectively.

As shown in Table 3, most defect-complexes have positive binding energies which indicates the tendency of forming a complex, but two cases show up with a very large negative binding energies. Interestingly, the negative binding energy only happens when the V_O and In_{Zn} defects are located in different atomic-layers. More interestingly, the binding energy of defect complex at sites O48−Zn21 is about 0.4 eV, but that of the defect complex at sites O48−Zn25 is about −0.6 eV, showing a difference as large as 1.0 eV. Remember that sites Zn21 and Zn25 are "quasi-equivalent" to each other for the In_{Zn} antisite defects, and our direct calculations told us the energy differences between these two systems with an isolated In_{Zn} at site Zn21 and Zn25, in both $q = 0$ and +1 charge states, are smaller than 0.0005 eV. Thus, we can guess that defect-complexes between V_O and In_{Zn} prefer the atomic sites in the same atomic layer in the (Zn/In)O slab. This bias results from relaxation of both the atomic structure and electronic structure, which actually should be correlated to each other.

Table 3. Total energies with respect to that of defect-complex consist of V_O at site O48 and In_{Zn} at Zn13 (δE_{tot}), and binding energy (E_b) of various defect-complex between V_O and In_{Zn} at different atomic sites as shown in Figure 3(a)

V_O−In_{Zn}	δE_{tot} (eV)		E_b (eV)	
Site labels	$q = 0$	$q=+1$	$q = 0$	$q=+1$
38−13	0.14	0.11	0.20	0.26
38−14	0.26	0.24	0.35	0.41
43−18	0.31	0.30	0.31	0.37
43-21	0.35	0.34	0.17	0.21
44−13	0.36	0.36	−0.54	−0.48
44−18	0.02	0.04	0.03	0.09
47−20	0.29	0.28	0.24	0.29
47−21	0.26	0.26	0.27	0.32
48−19	0.11	0.12	0.37	0.43
48−21	0.00	0.00	0.20	0.26
48−25[a]	0.85	0.83	−0.64	−0.60

[a]Site Zn25 is "quasi-equivalent" to Zn21.

From previous discussions, on one hand, the isolated neutral charged oxygen vacancy will push its apical Zn(5) away from the vacancy site, and this Zn(5) atom will try to restore the Zn−O tetrahedron structure; on the other hand, the isolated antisite In_{Zn} will try its best to enhance the In−O bipyramid structure by pulling its apical oxygen atoms toward itself. Thus, these two opposite relaxation patterns will compete with each other when such a V_O-In_{Zn} defect-complex is formed. From the fully relaxed structures of V_O-In_{Zn} defect-complexes, we found that the oxygen vacancy pushed the apical In_{Zn} away, and then the In_{Zn} atom forms an In(4)-O tetrahedron structure which is not favored by an indium atom. Besides, it costs more energy to relax the oxygen atoms around the In_{Zn} site to accommodate the large indium atom.

In Figure 5 (c), (d) and (e), we plot the site-projected density of states (PDOS) on the In_{Zn} and V_O sites for V_O-In_{Zn} defect-complexes with q=+1 at sites O48−Zn18, O48−Zn21, and O48−Zn25, respectively. PDOS for the isolated oxygen vacancy ($*V_O$) has also been plotted, the energy zero is set at the VBM of the perfect host, and the vertical dashed lines indicate the Fermi levels. Figure 5(c) and (d) show exactly what happens in the schematic diagram Figure 5(b): strong hybridization happens between the isolated V_O and In_{Zn} states which corresponds to the D1 and D2 states in Figure 5(b), and a bonding state is formed significantly below the isolated oxygen vacancy state. In contrast, these behaviors do not show up for the defect-complex at O48−Zn25 where the two sites are not in the same basal plane.

In conclusion, oxygen vacancies and indium antisite on zinc sites tend to form defect-complexes when they are nearest-neighbors in the same basal plane (or *ab*-plane). So the quite uniform spatial distribution of In_{Zn} will be strongly modified by the anisotropic spatial distribution of V_O. In the equilibrium case, we can expect that most of the defects will occur along the zigzag Zn−In−O boundary in the (Zn/In)O slabs in the $In_2O_3(ZnO)_k$ compounds.

A New Possible Explanation for the Anisotropic Electrical Conductivities. Experimental observations of the strong anisotropy in electrical conductivities were reported for thin-film[4] and single crystal[5] $In_2O_3(ZnO)_5$. Usually, it is believed that this anisotropic phenomenon is the reflection of a high anisotropy in the layered crystal structure.[5] However, in our previous study,[3] we found that the lowest conduction band of $In_2O_3(ZnO)_k$ with k = 1−3 are actually isotropic in three reciprocal lattice vector directions. In this study, we also investigated the band structures of phases with k = 4, and 5, and the conclusion remains correct. In $(InGa)ZnO_4$, the same contradiction has been described recently, and was explained by the anisotropic distribution of the metastable V_O^{1+} which was considered as the main carrier producer.[6] Here, we would like to claim that whatever the carrier sources, the electron carriers should be excited to the conduction band at first and then become conducting electrons. For $In_2O_3(ZnO)_k$ where In_{Zn}^{1+} or its complexes with V_O act as the carrier sources, the defect bands are located above the CBM, and the conducting electrons are populated in the lowest host conduction bands which are perturbed by the defects. In ZnO, and perhaps also $(InGa)ZnO_4$, where the photoexcited metastable V_O^{1+} act as the carrier sources, the excited electrons will also occupy the perturbed-host states[20,22] near the CBM. In both cases, if the lowest conduction bands of the pure host is highly isotropic,

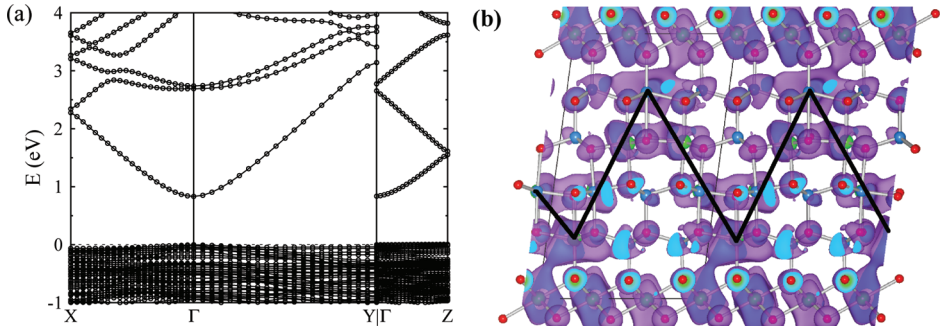

Figure 6. (Color-online) (a) The GGA band structure of $In_2O_3(ZnO)_3$, where X=(1/2, 0, 0), Y=(0, 1/2, 0), Z=(0, 0, 1/2); (b) isosurface plot of the squared electron wave function near the CBM.[16]

the effective mass (m^*) should be isotropic. $In_2O_3(ZnO)_3$ belongs to this kind of situation, as shown in Figure 6(a) where we plot the band structure of $In_2O_3(ZnO)_3$ from the GGA calculations.

Within the effective mass and relaxation time approximation, the electrical conductivity $\sigma=ne\mu=ne^2\tau/m^*$, where n, μ, τ, and m^* are the carrier concentration, and mobility, relaxation time, and effective mass, respectively. In the same sample, n is always the same,[5] and m^* is highly isotropic in $In_2O_3(ZnO)_k$, so the anisotropic electrical conductivities should result from an anisotropic relaxation time. The defects with high concentration, strong deformation potential, and Coulomb potential can largely reduce the relaxation time.[52] In $In_2O_3(ZnO)_k$, the concentration of In_{Zn} should be comparable with the carrier density, and the concentration of V_O should be much larger because of its lower formation energy compared with that of In_{Zn}, as shown in Figure 4. As discussed previously, most of these two kinds of defects will be located in the (Zn/In)O slab, while in the In−O layer there are much much less defects. Thus, the relaxation will shown high anisotropy with a much longer τ along the In−O layer than that along the normal direction out of the In−O layer.

To explain the extremely strong anisotropic behavior, which is of 2 orders of magnitude,[5] we plot the isosurface of the squared wave functions near the CBM in Figure 6(b). The squared wave function tells us that the conducting electrons have a larger probability to distributed in the In−O layer and along the zigzag boundary, which agree with a recent investigation with an improved description of the exchange-correlation.[36] So, the In−O layer should be the main in-plane conducting path, and the zigzag boundaries the main out-of-plane conducting path. In equilibrium conditions, the V_O tend to occur along the zigzag boundaries, and the In_{Zn} also tend to occurs along the zigzag boundaries by forming complexes with V_O. Thus, the main conducting path along the out-of-plane direction would be blocked due to the high concentration of scattering centers either with strong deformation potential[52] (V_O) or with strong Coulomb potential[52] (In_{Zn}) due to the low dielectric constant. All of these lead to the strongly anisotropic relaxation time, and therefore, to the strongly anisotropic electrical conductivities in $In_2O_3(ZnO)_k$.

SUMMARY

In this study, we calculate the defect formation energies and transition energy levels of several n−type defects at various atomic sites in $In_2O_3(ZnO)_3$ which is used as a case study for the series of homologous compounds $In_2O_3(ZnO)_k$ with k = integers. Oxygen vacancy (V_O), indium antisite on zinc (In_{Zn}), indium interstitial (In_i), and zinc interstitial (Zn_i) are fully considered, as well as some defect complex between V_O and In_{Zn} or Zn_i. According to the calculated formation energies, the most abundant defects should be V_O and In_{Zn}, among which In_{Zn} should be the possible intrinsic n−type carrier producer because of its shallow transition energy level, while V_O tends to not release the electrons. V_O has very strong site-preference, and therefore the anisotropic spatial distribution: most of V_O should take the sites along the zigzag boundary in the (In/Zn)O slab. The anisotropic spatial distribution of V_O will affect that of In_{Zn}, via forming defect complexes when the two defects take the nearest neighbor atomic sites in the same *ab*-plane. The electronic structure calculation show that the zigzag boundary is actually the main conducting path along the *c* direction. Thus, the anisotropic spatial distribution of the defects which act as scattering centers would lead to anisotropic relaxation time, and then strong anisotropy in electrical conductivities, although the band dispersion (effective mass) is highly isotropic.

ASSOCIATED CONTENT

Supporting Information

This material is available free of charge via the Internet at http://pubs.acs.org.

AUTHOR INFORMATION

Corresponding Author

*To whom correspondence should be addressed E-mail: haowei-peng@northwestern.edu.

ACKNOWLEDGMENTS

We thank Dr. Da Silva and Dr. Wei for their courtesy of providing the elaborated atomic structures of $In_2O_3(ZnO)_k$ with k = 1−6, and thank Dr. Lany for helpful discussion on the defect calculations. This work is supported by the U.S. Department of Energy, Office of Science, Office of Basic Energy Sciences under the Award Number DE-FG02-06ER46320, and also by the NSF-MRSEC at N.U. Materials Research Center.

REFERENCES

(1) Minami, T.; Kakumu, T.; Takata, S. *J. Vac. Sci. Technol. A* **1996**, *14*, 1704.
(2) Hoel, C. A.; Mason, T. A.; Gaillard, J.-F.; Poeppelmeir, K. R. *Chem. Mater.* **2010**, *22*, 3569.
(3) Hopper, E. M.; Zhu, Q.; Song, J.-H.; Peng, H.; Freeman, A. J.; Mason, T. O. *J. Appl. Phys.* **2011**, *109*, 013713.
(4) Hiramatsu, H.; Ohta, H.; Seo, W.-S.; Koumoto, K. *J. Jpn. Soc. Powder Powder Metall.* **1997**, *44*, 44.

(5) Malochkin, O.; Seo, W.-S.; Koumoto, K. *Jpn. J. Appl. Phys.* **2004**, *43*, L194.
(6) Medvedeva, J. E.; Hettiarachchi, C. L. *Phys. Rev. B* **2011**, *81*, 125116.
(7) Wei, S.-H. *Comput. Mater. Sci.* **2004**, *30*, 337.
(8) Van de Walle, C. G.; Neugebauer, J. *J. Appl. Phys.* **2004**, *95*, 3851.
(9) Li, C.; Bando, Y.; Nakamura, M.; Onoda, M.; Kimizuka, N. *J. Solid State Chem.* **1998**, *139*, 347.
(10) Yan, Y.; Pennycook, S. J.; Dai, J.; Chang, R. P. H; Wang, A.; Marks, T. J. *Appl. Phys. Lett.* **1998**, *73*, 2585.
(11) Schinzer, C.; Heyd, F.; Matar, S. F. *J. Mater. Chem.* **1999**, *9*, 1569.
(12) Dupont, L.; Maugy, C.; Naghavi, N.; Guery, C.; Tarascon, J.-M. *J. Solid State Chem.* **2001**, *158*, 119.
(13) Uchida, N.; Bando, Y.; Nakamura, M.; Kimizuka, N. *J. Electron Microsc.* **1994**, *43*, 146.
(14) Yan, Y.; Da Silva, J. L. F.; Wei, S.-H.; Al-Jassim, M. *Appl. Phys. Lett.* **2007**, *90*, 261904.
(15) Da Silva, J. L. F.; Yan, Y.; Wei, S.-H. *Phys. Rev. Lett.* **2008**, *100*, 255501.
(16) Momma, K.; Izumi, F. *J. Appl. Crystallogr.* **2008**, *41*, 653.
(17) Kasper, V. H. *Z. Anorg. Allg. Chem.* **1967**, *349*, 113.
(18) Zhang, S.-B.; Wei, S.-H.; Zunger, A. *Phys. Rev. B* **2001**, *63*, 075205.
(19) Janotti, A.; Van de Walle, C. G. *Appl. Phys. Lett.* **2005**, *87*, 122102.
(20) Lany, S.; Zunger, A. *Phys. Rev. B* **2005**, *72*, 035215.
(21) Lany, S.; Osorio-Guillén, J.; Zunger, A. *Phys. Rev. B* **2007**, *75*, 241203(R).
(22) Lany, S.; Zunger, A. *Phys. Rev. Lett.* **2007**, *98*, 045501.
(23) Oba, F.; Togo, A.; Tanaka, I.; Paier, J.; Kresse, G. *Phys. Rev. B* **2008**, *77*, 245202.
(24) Lany, S.; Zunger, A. *Phys. Rev. B* **2008**, *78*, 235104.
(25) Ágoston, P.; Albe, K.; Nieminen, R. M.; Puska, M. J. *Phys. Rev. Lett.* **2009**, *103*, 245501.
(26) Ágoston, P.; Erhart, P.; Klein, A.; Albe, K. *J. Phys.: Condens. Matter.* **2009**, *21*, 455801.
(27) Clark, S. J.; Robertson, J.; Lany, S.; Zunger, A. *Phys. Rev. B* **2010**, *81*, 115311.
(28) Lany, S.; Zunger, A. *Phys. Rev. B* **2010**, *81*, 113201.
(29) Tomita, T.; Yamashita, K.; Hayafuji, Y.; Adachi, H. *Appl. Phys. Lett.* **2005**, *87*, 051911.
(30) Kim, Y.-S.; Park, C. H. *Phys. Rev. Lett.* **2009**, *102*, 086403.
(31) Tang, L.-M.; Wang, L.-L.; Wang, D.; Liu, J.-Z.; Chen, K.-Q. *J. Appl. Phys.* **2010**, *107*, 083704.
(32) Nakamura, M.; kimizuka, M.; Mohri, T. *J. Solid. State Chem.* **1990**, *86*, 16.
(33) Kimizuka, N.; Isobe, M.; Nakamura, M. *J. Solid. State Chem.* **1994**, *116*, 170.
(34) Moriga, T.; Edwards, D. D.; Mason, T. O.; Palmer, G. B.; Poeppelmeier, K. R.; Schindler, J. L.; Kannewurf, C. R.; Nakabayashi, I. *J. Am. Ceram. Soc.* **1998**, *81*, 1310.
(35) Moriga, T.; Fukushima, A.; Tominari, Y.; Hosokawa, S.; Nakabayashi, I.; Tominaga, K. *J. Synchrotron Rad.* **2001**, *8*, 785.
(36) Walsh, A.; Da Silva, J. L. F.; Yan, Y.; Al-Jassim, M. M.; Wei, S.-H. *Phys. Rev. B* **2009**, *79*, 073105.
(37) Perdew, J. P.; Burke, K; Ernzerhof, M. *Phys. Rev. Lett.* **1996**, *77*, 3865.
(38) Blöchl, P. E. *Phys. Rev. B* **1994**, *50*, 17953.
(39) Kresse, G.; Hafner, J. *Phys. Rev. B* **1993**, *48*, 13115. Kresse, G.; Furthmüller, J. *Phys. Rev. B* **1996**, *54*, 11169. Kresse, G.; Joubert, D. *Phys. Rev. B* **1999**, *59*, 1758.
(40) Monkhorst, H. J.; Pack, J. D. *Phys. Rev. B* **1976**, *13*, 5188.
(41) Persson, C.; Zhao, Y. J.; Lany, S.; Zunger, A. *Phys. Rev. B* **2005**, *72*, 035211.
(42) Liechtenstein, A. I.; Anisimov, V. I.; Zaane, J. *Phys. Rev. B* **1995**, *52*, R5467.
(43) Heltemes, E. C.; Swinney, H. L. *J. Appl. Phys.* **1967**, *38*, 2387.
(44) Hamberg, I.; Granqvist, C. G. *J. Appl. Phys.* **1986**, *60*, R123.
(45) Rinke, P.; Janotti, A.; Scheffler, M.; Van de Walle, C. G. *Phys. Rev. Lett.* **2009**, *102*, 026402.
(46) Walsh, A.; Catlow, C. R. A.; Miskufova, M.; Sokol, A. A. *J. Phys.: Condens. Matter.* **2011**, *23*, 334217.
(47) Walsh, A.; Sokol, A. A.; Catlow, C. R. A. *Phys. Rev. B* **2011**, *83*, 224105.
(48) Scanlon, D. O.; Walsh, A.; Watson, G. W. *Chem. Mater.* **2009**, *21*, 4568.
(49) Da Silva, J. L. F.; Walsh, A.; Lee, H. *Phys. Rev. B* **2008**, *78*, 224111.
(50) Osorio-Guillén, J.; Lany, S.; Barabash, S. V.; Zunger, A. *Phys. Rev. Lett.* **2006**, *96*, 107203.
(51) Note: all these inspection are based on the structure models provided by Da Silva et.al.[15]
(52) Blic, D. I.; Mahanti, S. D.; Kanatzidis, M. G. *Phys. Rev. B* **2006**, *74*, 125202.